



Article

Fractographic Investigation of Cryogenic Temperature Mode-II Delamination Behavior of Filament Wound CFRP Laminates with Varied Resin Systems

Recep Ufuk ¹, Kaan Bilge ^{2,*}, Barış Emre Kırıl ³, Murat Ereke ¹ and Arif Karabeyoğlu ⁴

¹ Faculty of Mechanical Engineering, Istanbul Technical University, 34437 Istanbul, Turkey; ufuk@itu.edu.tr (R.U.); ereke@itu.edu.tr (M.E.)

² Insight Technology Development and Consultancy, 34742 Istanbul, Turkey

³ Faculty of Engineering and Natural Sciences, Sabanci University, 34956 Istanbul, Turkey; bekiral@sabanciuniv.edu

⁴ Faculty of Mechanical Engineering, Koç University, 34450 Istanbul, Turkey; akarabeyoglu@ku.edu.tr

* Correspondence: kaanbilge@insighttech.info

Abstract: This study investigates the mode-II delamination performance of filament-wound unidirectional composites with different types of epoxies as their matrix phase under room and cryogenic temperatures. A typical vacuum infusion resin, an aerospace-grade cold-curing resin and crack-resistant toughened resin systems were wet-wound with 12K carbon fiber tows to manufacture the composite samples. Test samples with a (0)₁₆ ply sequence were tested according to ASTM D7905-19. The tested samples were investigated via microscopic analysis to assess the failure mechanisms associated with varying the matrix material and temperature. ENF tests at room temperature were found to be susceptible to the inherent variance in the fiber architectures along with resin-viscosity-driven fiber wetting. Cryogenic conditions induce a shift in the mode-II delamination behavior from a rather complex failure mechanism to a consistent fiber/matrix debonding mode with diminishing G_{IIc} values except for the toughened resin system. The provided comprehensive fractographic analysis enables an understanding of the various causes of fracture, which determines the laminate performance. The combined evaluation of the distinctive damage modes reported in this study provides guidance on the conventional wet-winding process, which still remains a volumetrically dominant and viable option for cryogenic applications, particularly for vessels with limited operational durations like sounding rockets.

Keywords: cryogenic; CFRP; filament-wound; delamination; end-notched flexure; mesoscale; mode II; fractography; SEM; tow undulation



Citation: Ufuk, R.; Bilge, K.; Kırıl, B.E.; Ereke, M.; Karabeyoğlu, A. Fractographic Investigation of Cryogenic Temperature Mode-II Delamination Behavior of Filament Wound CFRP Laminates with Varied Resin Systems. *J. Compos. Sci.* **2023**, *7*, 450. <https://doi.org/10.3390/jcs7110450>

Academic Editors: Francesco Tornabene and Salvatore Brischetto

Received: 7 September 2023

Revised: 10 October 2023

Accepted: 23 October 2023

Published: 30 October 2023



Copyright: © 2023 by the authors. Licensee MDPI, Basel, Switzerland. This article is an open access article distributed under the terms and conditions of the Creative Commons Attribution (CC BY) license (<https://creativecommons.org/licenses/by/4.0/>).

1. Introduction

The high demands of the aerospace and automotive industries have resulted in the need to develop linerless composite pressure vessels due to their potential weight reduction. The weakest links for any composite structure are matrix-related micro-crack formation and accumulation, which may cause leakage problems and pressure-bearing capacity losses in the vessel even at room temperature [1,2]. At cryogenic temperatures, the observation and understanding of the thermomechanical response of matrix- and matrix/fiber-interface-driven failure modes becomes even more important [3–5].

The development of composite pressure vessels requires a combined systematic approach, including composite laminate design, modelling, material testing and large-scale manufacturing.

Modelling studies focus on a multi-scaled approach, where constitutive relationships are of concern at different length scales and are frequently studied using finite element analysis [6,7]. The aim here is to deduce the vessel performance in order to (i) choose the

constituents at the microscale [8], (ii) reinforce the tow architectures at the mesoscale [4,5] and (iii) design related responses of vessels at the macroscale [9]. In addition to the mechanical response, works investigating methods for determining the permeation rate and for software development have also been reported [10]. Parallel to modelling efforts, experimental studies share the multi-scaled approach and focus on large-scale composite vessel manufacturing/testing, specimen-based laminate testing and constituent testing in a cryogenic environment.

At the macroscale, studies on cryogenic composite pressure vessel have been focused on the permeability characteristics under cryogenic conditions. Some of the most recent works were presented by Flanagan et al. [11], who studied the cryogenic cycling effect on the permeability of PEEK matrix composite pressure vessels considering variations in the pressure, thickness, fiber and matrix type. Grogan [12] worked on the damage and permeability of tape-laid thermoplastic composite tanks experimentally and numerically. Yokozeki [13] evaluated helium leakage on carbon-fiber-reinforced plastic (CFRP) tubes by applying tensile loading to the composite tubes at room temperature (RT) and at cryogenic liquid nitrogen (LN₂) temperature.

At the microscale, the constituent thermomechanical properties are also profoundly significant in improving the composite laminate response under cryogenic conditions, especially for matrix materials. For this reason, many research studies have been conducted and continue to be carried out to understand the contribution of matrices to the mechanical response of composite laminates. One of the leading areas of focus on matrix materials is toughened epoxy systems for cryogenic environments. Their molecular movement capability under cryogenic conditions provides improved fracture toughness values, again under cryogenic conditions. This behavior is explained by the “free volume-free space” theory [14]. The general trend in the literature is toward toughening epoxy systems with additives/fillers such as MWCNT [15], graphene platelets and rubbery particles [16–18]. Liu et al. [19] reported that the addition of nanosheet boehmite (AlOOH) provides an increase in the interlaminar fracture toughness under room-temperature conditions; however, it provides no improvement under cryogenic temperatures. The filler type and weight ratio are critical for property maximization, and the optimal values can differ for room-temperature and cryogenic conditions [20,21]. The chemical toughening method represents another method for cryogenic environments, and it reduces transverse cracking under cryogenic conditions [5,22,23]. Coronado et al. [22] studied the low-temperature fatigue resistance of untoughened and toughened matrix systems and reported the favorable effect of toughening on mode-I fatigue resistance. Also, damage morphologies such as river markings, broken fibers and hackle patterns have been reported. However, transverse cracking of chemically toughened epoxy systems under cryogenic conditions has not been reported at the meso-mechanical scale with fractographic images.

The effect of manufacturing parameters such as the fiber width and fiber undulation parameters on the mechanical properties and damage modes of composite laminates has also been investigated theoretically [24–26]. Numerical analyses have also focused on the meso-scale effects of fiber undulations and winding patterns [27–29]. One recent study conducted with a three-dimensional (3D) repeated unit cell (RUC) at the mesoscale by Pourahmadi [30] indicates that fiber bundle crossovers and undulations can change the mechanical and thermal properties by up to 15.7% when compared to the composite lamination theory. Shen et al. [31] also investigated the effects of fiber crossover and undulation on stiffness failure using numerical and analytical calculations, and they point out that the strain levels are higher by about 1.07–1.13 times in the undulation regions compared to the laminate regions. However, all these works are based on mesoscale winding pattern analysis and do not discuss tow undulation effects at the microscale level.

Fracture toughness measurements to assess crack formation and propagation in composite structures have thus become a challenging task due to the above-stated variances in the different length scales. Such effects have been thoroughly investigated at room temperature for several composite structures. Barcikowski and Rybkowska [32] studied

the characterization of reactive rubber-added toughened epoxy resins. Rased [33] studied the asymmetrical stacking sequence effect on the fracture toughness values of carbon fiber composites via double-cantilever beam (DCB), end-notched flexure (ENF) and mixed-mode bending (MMB) tests. Morais [34] worked on the mode-II behavior of angle-ply glass/polyester filament-wound specimens. Bonhomme et al. [35] investigated the mode-I and mode-II interlaminar fracture surfaces of a unidirectional AS4/8552 carbon/epoxy laminate with fractographic and numerical analyses at room temperature.

Studies on fracture toughness testing under cryogenic temperatures remain rather unexplored when compared with RT testing efforts. Micro-crack progression was investigated by Li et al. [36], who discussed the effect of flexible molecular-structured epoxy on the cryogenic mechanical performance of the matrix and CFRP laminates with tensile and flexural tests under both room-temperature and cryogenic temperatures. Shindo [10] studied the delamination growth of woven glass-reinforced epoxy with mode-II fatigue loadings and four-point ENF tests at cryogenic temperatures. Choi and Sankar [37] performed four-point bending tests on single-notched graphite–epoxy laminates at room and cryogenic temperatures. Although these works have provided exemplary approaches, the current state of the art lacks an experimental approach where resin (*ex situ*) and laminate (*in situ*) testing are simultaneously performed. Moreover, the presented fractographic analyses have focused on explaining selected laminate behaviors rather than the effect of the resin choice and how the corresponding fracture mechanisms are affected under cryogenic environments.

Originating from this point, this article aims to highlight the effect of the resin type and manufacturing-related anomalies, such as resin bagging, fiber undulations and fiber wetting, on the mode-II delamination behavior of wet-wound UD composite specimens. Specific attention is given to the fractographic identification of such anomalies, which is of utmost importance for the failure analysis of composite pressure vessels. Three different resin systems were used for neat epoxy tests and for manufacturing CFRP laminate: low-viscosity cold curing (CC), low-viscosity warm-to-hot curing (VI) and toughened epoxy systems (T). Conventional filament winding by a four-axis winding machine was employed. The ENF specimens were prepared from $(0)_{16}$ laminates, which were manufactured by filament winding on a flat mandrel. The specimens were tested for their mode-II strain energy release rates (G_{IIc}) under RT and cryogenic (LN2) conditions. The modes of failure on the filament-wound CFRP laminates manufactured with different resin types and the effect of the temperature on the resin morphologies were investigated by detailed fractography analyses for each scenario. This thorough examination of these fracture surfaces provides a comprehensive understanding of the complex interaction between the behavior of epoxy systems and the damage mechanisms that arise within intricate mesoscale-architecture filament-wound composite laminates.

2. Materials and Methods

2.1. Materials

Three different DGBEA epoxy systems were used for this study. The first one, MARKUT 5025 (CC resin), was an aerospace cold-curing system, and the second one, BASAT 11546 (warm-to-hot-curing vacuum-infusion resin system) (VI resin), was purchased from CET Epoksi Teknolojileri A.Ş. (Istanbul, Turkey). The third one, CTD 7.1 Toughened Epoxy Resin (T resin), was a high-microcrack-fracture-toughness cryogenic resin system purchased from Composite Technology Development Inc. (Lafayette, LA, USA). Specific attention was given to the viscosity values to ensure that the chosen resin types were suitable for the filament-winding process. The characteristics of the purchased resin samples are shown in Table 1.

A-49 12K tow carbon fiber was purchased from Dow-Aksa (Istanbul, Turkey) and used for manufacturing the CFRP laminates (Figure 1).

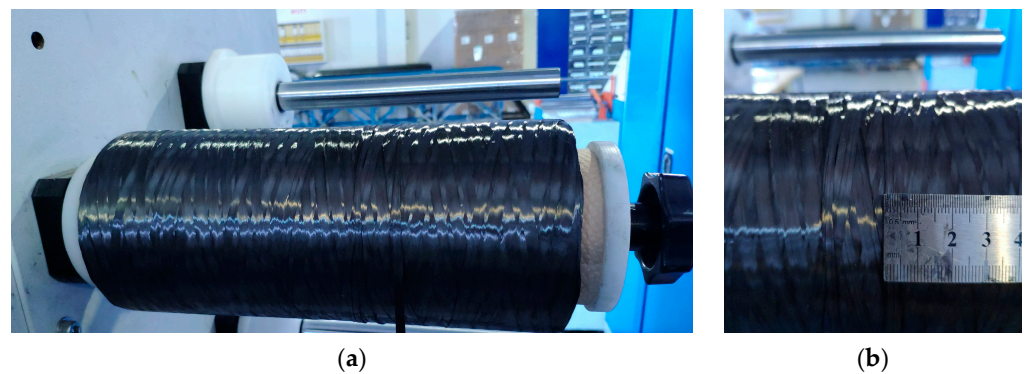


Figure 1. (a) Carbon fiber tow; (b) carbon tow bandwidth.

Table 1. Epoxy systems, pot life, curing cycle and viscosity properties.

| Epoxy System | Pot Life at 23 °C (hours) | Nominal Curing Cycle | Resin Viscosity (cPs) | Hardener Viscosity (cPs) | Measured T_g * (°C) | Data Sheet T_g (°C) |
|---|---------------------------|----------------------------|-----------------------|--------------------------|-----------------------|-----------------------|
| MARKUT 5025 (CC resin) | 2–3 | 1 day 23 °C+ 4 h 100 °C | 1000–1500 at 5 °C | 40–60 at 25 °C | 98.8 | 118–124 |
| BASAT 11546 (VI resin) | 4.5 | 1 h 80 °C+ 4 h 120 °C | 1200–1400 at 25 °C | 10–30 at 25 °C | 109.3 | 115–120 |
| CTD 7.1 Toughened Epoxy Resin (T resin) | 3.5 | 2 h 80 °C | 1500–5000 at 50 °C | 12 at 25 °C | 66.3 | 80 |

* Measurements were obtained from manufactured ENF samples.

The selected resin systems exhibited significant viscosity differences, which was attributed to both the resin and hardener viscosities, with the VI resin system having the lowest mixture viscosity and the T system exhibiting the highest mixture viscosity.

2.2. Specimen Preparation

First, neat epoxy samples were prepared for both room-temperature and cryogenic testing. Before the stoichiometric mixing, all samples were gently mixed for 15 min to enhance the homogeneity of the resin, hardener and initiator components. These mixtures were then introduced into silicon molds shaped according to ASTM D790-17 [38]. The curing of the samples took place in a temperature- and humidity-controlled oven, following the recommended curing specifications provided by the manufacturers (as outlined in Table 1). The T_g values from the in-house manufactured samples fell within an acceptable range when considering the scale of production.

ENF test specimens were manufactured in accordance with ASTM D7905/D7905M-19 [39] (Figure 2). The filament winding of the (0)₁₆ UD laminates was carried out using a specially designed mandrel following the ISO 1268-5 [40] guidelines. The winding process employed a single row of fiber with a 3.1 mm bandwidth (Figure 3a). The winding tension was set to 20 N, and the average winding speed was 15 rpm. Four hoop layups were wound, and a 12 μ m Teflon-based insert material was placed at both ends of the mandrel (Figure 3b). Subsequently, four additional hoop layups were added to create a symmetrical and balanced laminate. The CFRP specimens were then obtained from the manufactured laminates through water jet cutting, as illustrated in Figure 3c, highlighting the undulations caused by the filament-winding process.

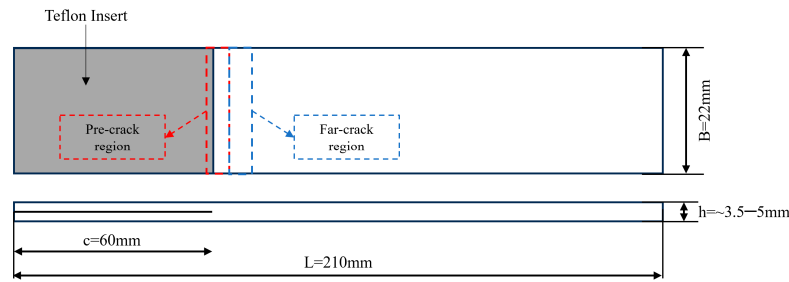


Figure 2. ENF specimen dimensions (dashed line regions represent investigated fracture regions).

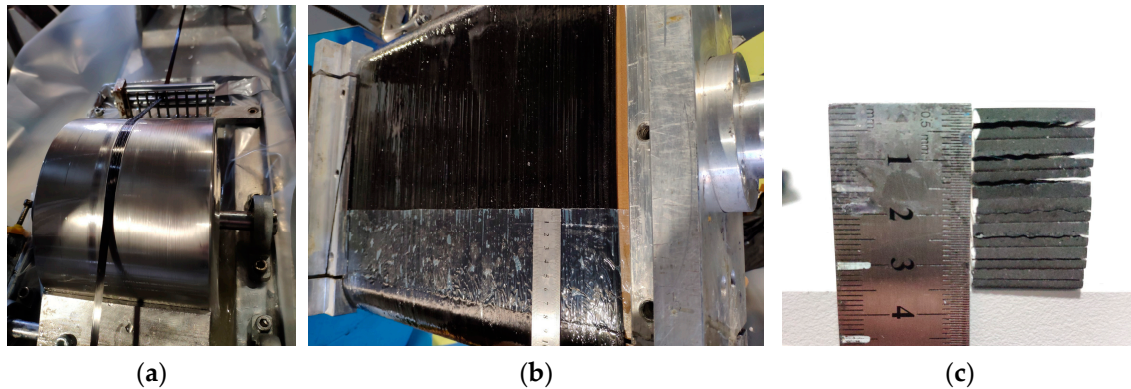


Figure 3. (a) One row of tow; (b) filament-winding process; (c) cross-section view of ENF specimens.

2.3. Mechanical Tests

Initial attention was directed towards conducting cryogenic tests on the neat epoxy samples to investigate the connection between the self-behavior and the in-situ behavior of the selected resins.

Three-point bending tests were conducted on the neat epoxy samples to assess their mechanical responses under both room-temperature and cryogenic conditions. Both the cryogenic and room-temperature three-point bending tests on the cast epoxy samples adhered to the ASTM D790 [38] standards and were performed using a 10 kN Shimadzu AGS-X universal testing machine (Kyoto, Japan) at a crosshead displacement rate of 5mm/min. The force-versus-displacement values were recorded for the subsequent calculations of the parameters including the maximum flexural strain (ϵ_{max}), maximum flexural stress (σ_{max}) and E_{flex} flexural modulus. These parameters were determined using the following formulas:

$$\sigma_{max} = \frac{3FL}{2Bd^2} \tag{1}$$

$$\epsilon_{max} = \frac{6Dd}{L^2} \tag{2}$$

$$E_{flex} = \frac{FL^3}{2BDd^3} \tag{3}$$

where F represents the maximum recorded force in the force–displacement curves, L is the half-span length, B is the specimen width, d is the thickness of the sample and D is the deflection of the beam center [38]. A minimum of eight specimens were tested for each case.

For the ENF tests, the same three-point bending fixture was employed, maintaining a constant crosshead displacement rate of 5 mm/min. Consequently, the non-precracked G_{IIc} values were calculated based on the direct beam theory, as reported in [41]. The formula for calculating G_{IIc} is as follows:

$$G_{IIc} = \frac{9a^2P\delta}{2b(2L^3 + 3a^3)} \quad (4)$$

where P represents the maximum force, δ is the maximum displacement, a is the delamination crack length, b is the specimen width and L is the span length. Both RT and LN2 tests were carried out (See Figure 4).



Figure 4. ENF test performed in (a) RT environment; (b) LN2 environment.

The room-temperature tests were conducted in an environment with a temperature variation ranging from 20–25 °C, while the cryogenic tests involved submerging the specimen in liquid nitrogen (LN2). The LN2 temperature was measured with a thermocouple and maintained at -196 ± 1 °C. Prior to testing in LN2, the specimens were pre-cooled using boiled liquid nitrogen to prevent any thermal shock.

2.4. Microscopy

The tested ENF specimens were examined from their sides to observe the nature of the cracking events resulting from the temperature change.

Fracture surface analysis of the ENF samples was performed using a Zeiss LEO Supra VP35 (Oberkochen, Germany) field emission scanning electron microscope (SEM) (Sabanci University, Istanbul, Turkey). Prior to the analysis, a thin conductive Au/Pd coating was sputter-deposited onto the samples. The samples collected from both the end of the insert and the fracture surface were investigated in two distinct regions: the pre-crack front (crack initiation zone) and the far regions (crack propagation zone). This allowed for observations and comments on the differences in the crack initiation and propagation during the testing. The examination of the fracture surfaces was conducted in the secondary electron mode with a gun voltage of 5 kV.

3. Results

3.1. Three-Point Bending Tests

Figure 5 depicts the representative flexural stress/strain curves obtained from the neat epoxy sample tests, revealing a transition from elastoplastic behavior at room temperature to fully elastic behavior at cryogenic temperatures. The overall results are summarized in Table 2. When exposed to cryogenic conditions, the increase in E_{flex} for all three resin systems was approximately 280–400%, which was primarily due to embrittlement. Similarly, the strength values also showed an increase under cryogenic conditions for all three systems when compared to the room temperature values. However, the maximum elongation values exhibited a significant decrease when transitioning to cryogenic levels. This observation suggests that the chain mobility of the resin systems was reduced, leading to a corresponding increase in the intermolecular binding forces. These changes directly influenced the measured E_{flex} and elongation values [42–45].

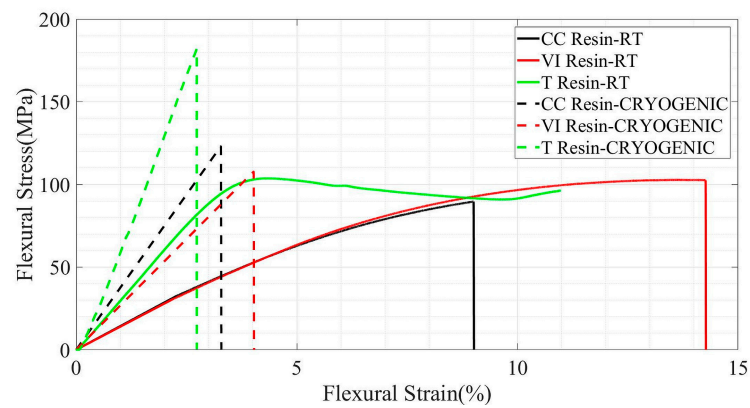


Figure 5. Representative flexural stress–strain curves of three-point bending tests of neat epoxy.

Table 2. Three-point bending and ENF results of epoxy specimens at room and LN2 temperatures.

| Resin Type | Test Environment | σ_{flex} | ϵ_{flex} | E_{flex} | G_{IIc} (kJ/m ²) | Vf |
|------------|------------------|-----------------|-------------------|----------------|--------------------------------|------|
| | | (MPa) | (%) | (MPa) | | |
| CC Resin | RT | 83.4 ± 8.8 | 8.4 ± 1.6 | 1012.2 ± 123.1 | 1.74 ± 0.17 | 0.5 |
| | LN2 | 139.7 ± 32.7 | 3.8 ± 0.9 | 3643 ± 63.2 | 0.88 ± 0.05 | |
| VI Resin | RT | 100.5 ± 3.7 | 13.2 ± 1.1 | 764.8 ± 61.1 | 0.97 ± 0.21 | 0.55 |
| | LN2 | 146.1 ± 26.0 | 4.6 ± 0.8 | 3180.2 ± 89.6 | 0.94 ± 0.08 | |
| T Resin | RT | 101.8 ± 6.8 | 4.7 ± 0.4 | 2243.0 ± 322.0 | 1.27 ± 0.09 | 0.45 |
| | LN2 | 170.9 ± 28.2 | 2.7 ± 0.3 | 6331.7 ± 578.2 | 1.22 ± 0.12 | |

The toughened resin system (T resin) exhibited remarkable toughness during the room-temperature test, enduring the test fixtures when they made contact, which serves as a clear demonstration of the positive toughening effect. However, the toughness effect was lost under cryogenic conditions, and the resin became brittle. This temperature-induced brittleness effect was also observed in the CC resin and VI resin systems. An intriguing point to note is that the E_{flex} value of the toughened resin system under room-temperature conditions was closely comparable to the cryogenic-temperature E_{flex} values of the other resin systems. The T system was the system most affected by the cryogenic temperatures, as it exhibited the highest strength value and the lowest strain among all the other resins under cryogenic conditions.

3.2. End-Notched Flexure Tests

Figures 6 and 7 display the representative force–elongation and flexural-stress–flexural-strain curves of the tested ENF specimens, respectively. The G_{IIc} values for the CC resin system were measured as 1.74 ± 0.17 (kJ/m²) at room temperature and 0.88 ± 0.05 (kJ/m²) at cryogenic temperature. In contrast, such a substantial decrease in the G_{IIc} values was not observed for the VI and T resins (Table 2). The room-temperature G_{IIc} level for the VI resin was 0.97 ± 0.21 (kJ/m²), while the cryogenic-temperature G_{IIc} level was 0.94 ± 0.08 (kJ/m²). For the T resin system, the force–elongation curve exhibited a remarkable similarity under both room and cryogenic conditions, with G_{IIc} values of 1.268 ± 0.091 (kJ/m²) and 1.216 ± 0.121 (kJ/m²) being obtained, respectively. The rationale behind the measured G_{IIc} values is discussed in more detail in the following section on the fractographic analysis.

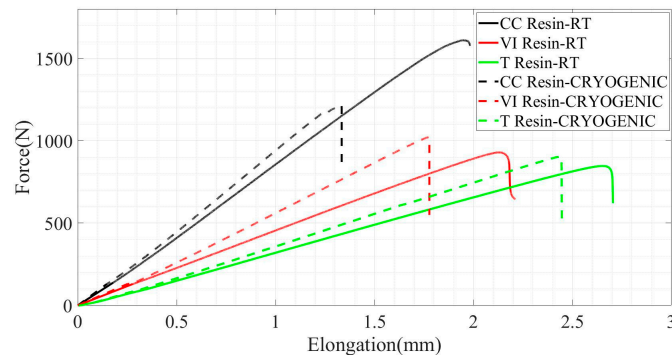


Figure 6. Representative force–elongation curves of ENF specimens.

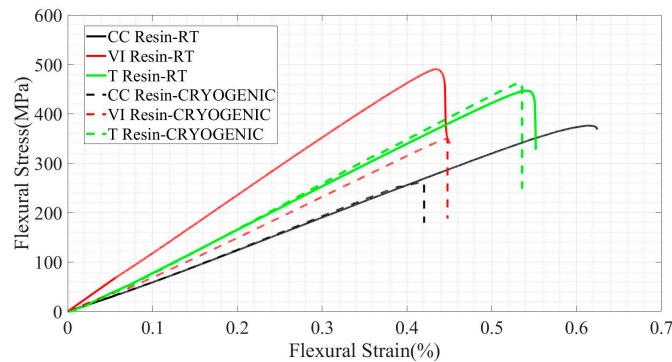


Figure 7. Representative flexural-stress–flexural-strain curves of ENF specimens.

4. Discussion

4.1. Macro-Scale Interpretation of the Main Mode of Failure

The effect of tow undulation was evident from the cross-sectional views of the tested specimens, as shown in Figure 2c. The side view of the tested specimens (Figure 8) revealed a linear crack propagation pattern at room temperature, which was replaced with a zig-zag crack propagation under LN2 conditions. The linear crack propagation was somewhat expected from the ENF tests due to the propagation of a mode-II crack along the interlaminar plane [33]. The periodic zig-zag crack propagation in the LN2 environment, on the other hand, suggests the coexistence of intra- and interlaminar damage propagation. The reduction in the G_{IIc} values, along with the presence of intra-laminar cracking, clarified the dominant mode of failure as fiber/matrix debonding under LN2 conditions due to the extreme cold affecting the regular resin types. These observations are linked to the significant difference in the thermal expansion coefficients between the tested resins and carbon fibers [10,36,37].

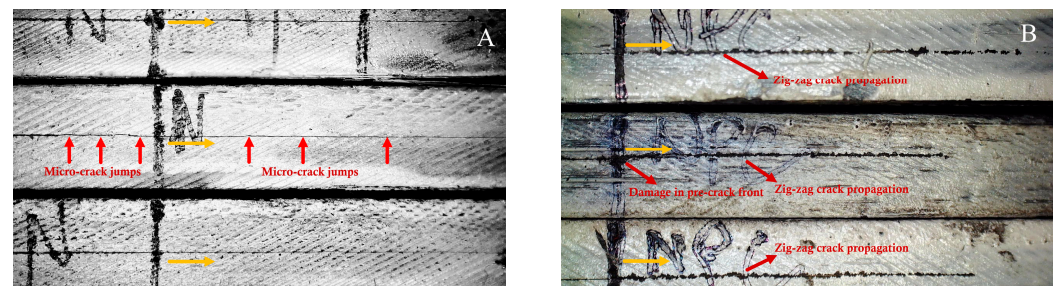


Figure 8. Side views of tested specimens (orange arrows indicate crack propagation direction): (A) CFRP-CC resin at RT with linear crack propagation; (B) CFRP-CC resin at LN2 with zig-zag crack propagation.

4.2. Crack Propagation Surfaces and Resin Morphologies

4.2.1. Pre-Crack Region (Crack Initiation Zone)

Pre-crack insertion during conventional filament winding can be rather challenging when compared to other mold-based manufacturing techniques (e.g., pre-preg laying, RTM). In this process, the entire manufacturing operation must be temporarily halted, and pre-cut non-sticking films need to be introduced at the crack-initiation regions on one part of the flat mold. During this pause, the amount of liquid resin on the pre-tensioned carbon fibers can change due to variations in the resin viscosities. As the process is continuous, the tows subjected to this interruption form the upper part of the interlaminar region. Consequently, the amount of resin on the interlaminar plane may vary, leading to the occurrence of resin bagging [22]. To illustrate this effect, the pre-crack fronts of the selected samples were analyzed using SEM.

The primary characteristic observed on the pre-crack fronts of all three types of samples that fractured at room temperature was the presence of resin bagging (Figure 9A–C). This issue led to the formation of periodic tow undulation. The undulated tow structure created hills on the fracture surface, resulting in non-planar mode-II crack propagation. This, in turn, left nearly perpendicular shear cusps at the side of the hills and caused simultaneous fiber/matrix debonding to occur on the plateau. The damage shape of the matrix was determined by the local stress state and the orientation of the hackles, indicating the direction of crack propagation [46]. For the toughened T resin system, local out-of-plane crack deflections revealed instances of crack jumping to other planes, and non-uniform crack initiation occurred at the crack front. These characteristics are unique to the conventional filament-winding process [30,31,33].

On the far region of the same undulated tow (Figure 9A–C), larger hackle formations characteristic of mode-II crack propagation and fiber/matrix debonding regions were demonstrated for the variance in the resin volume fraction along the interlaminar plane. The fundamental reason for this was determined to be the limited control of the perpendicular resin flow and tow overlapping [47,48] during the wet-winding process. In the investigated cases, the resin flow problem was even more problematic due to the pre-crack sticking-film-insertion process, where a total process stop was required.

For cryogenic conditions, the surface view was mostly flat and smooth, which suggests fiber/matrix debonding without any plastic deformation (Figure 9D,E). The effect of tow undulations was minor. However, again, for the toughened case, matrix hackle patterns and fiber/matrix debonding damage modes can be seen together. Also, the tow misalignment suggests that the tow movement was still effective for this toughened resin system due to the sample's plastic deformation capability under cryogenic conditions (Figure 9F).

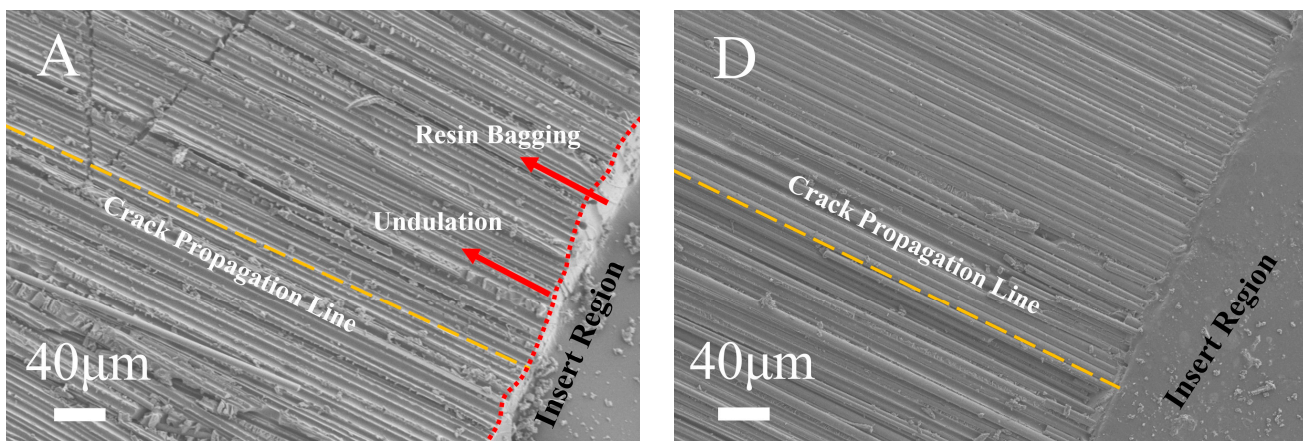


Figure 9. Cont.

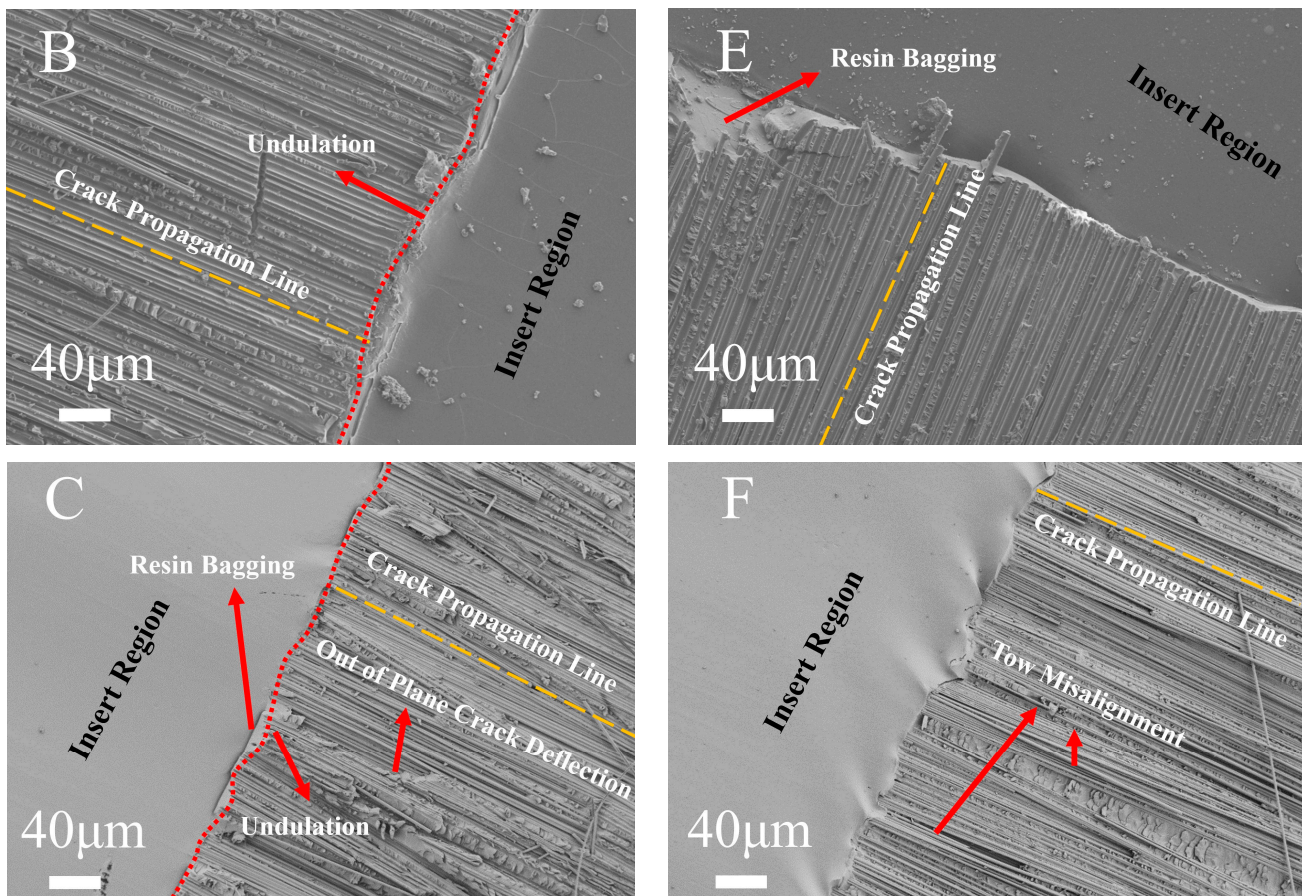


Figure 9. Fractographs belonging to the pre-cracked region of tested ENF samples; left shows RT sample: (A) CFRP-CC resin; (B) CFRP-VI resin; (C) CFRP-T resin. Right shows LN2 sample: (D) CFRP-CC resin; (E) CFRP-VI resin; (F) CFRP-T resin.

4.2.2. Far-Crack Region (Crack Propagation Zone)

Low-magnification images of the fracture surfaces of the investigated samples are presented for all three specimen types in Figure 10. A fundamental difference in the CFRP-VI resin laminate was the lower fiber wettability observed on the delamination surface. In contrast, the size and quantity of the hackle patterns (serrations) [46] on the CFRP-CC resin and CFRP-T resin surfaces were notably greater than those observed in the CFRP-VI resin laminate. This discrepancy accounts for the variations in measured G_{IIc} values at room temperature. Another valuable observation was the coexistence of interlaminar delamination (leaving hackle marks in between the continuous fibers) and fiber/matrix debonding failure events for all three types of specimens (as highlighted in Figure 10A,C,E). The continuous carbon fiber surfaces of the CFRP-CC resin laminates appeared relatively smoother when compared to CFRP-VI resin, indicating poorer fiber/matrix adhesion in the former. In contrast, the T resin system exhibited regions of the fiber/matrix interface that were well preserved, indicating strong fiber/matrix adhesion. Even in cases of fiber breakage, the presence of strong fiber/matrix adhesion was evident, leading to fiber rupturing (Figure 10E).

Furthermore, the presence of perpendicular hackle patterns (Figure 10A) suggests that the meso-structure resulting from the winding process induced non-planar crack propagation. This, in turn, led to an increase in the measured G_{IIc} values due to the tow interlocking effect. The frequency of such patterns was relatively lower in the case of the CFRP-VI resin (Figure 10C). When zoomed in (Figure 10B), the morphology of hackle patterns revealed that the in-situ behavior of the CC resin was much more ductile when compared to the VI resin. This is in contrast with the three-point bending results (Table 2).

This contradiction suggests that the higher strain values measured for the CC resin system during the ENF testing (Figure 7) were mainly due to the low fiber volume fraction ratio and also the undulations in the tow structures, whose movement was enabled at room temperature. On the other hand, the fiber/resin interaction was much more favorable in the case of the VI resin and the CC resin, where the surfaces of the carbon fibers were not as smooth, which caused a lower effect on the mode-II crack propagation (Figure 10D,E). The toughened system's resin damage morphology showed crack deflection in the investigated region (Figure 10F). The toughness effect revealed its contribution to the damage mode of the resin system due to the strong fiber/matrix adhesion and high shear deformation capability (Figure 10F).

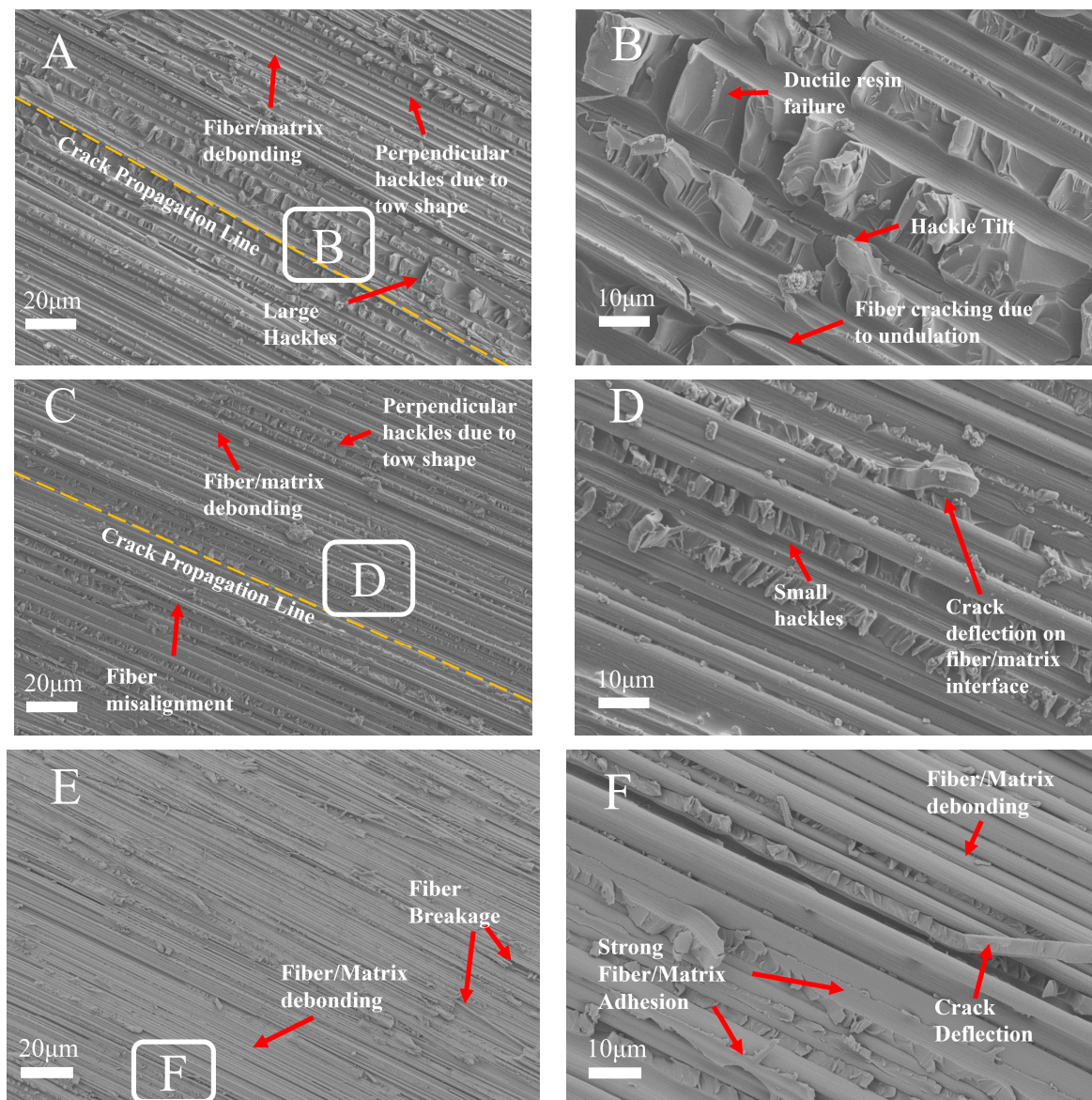


Figure 10. Fractographs belonging to tested ENF samples at RT (A); (B) CFRP-CC resin system (C); (D) CFRP-VI resin system (E); (F) CFRP-T resin system.

4.2.3. Effect of LN2 on Multi-Scaled Interactions

In contrast to the tests conducted at room temperature, the quantity of resin failure marks on the samples at cryogenic temperatures was notably smaller and less densely distributed, indicating that resin failure and tow undulations had a reduced impact on the fracture of the CC resin system (Figure 11A). Consequently, the zig-zag crack propa-

gation (Figure 7B) observed on the macroscale was primarily attributed to fiber/matrix debonding. However, in the case of the toughened resin system, the rate of resin failure was significantly higher on the damaged surface, where the resin remained effective under cryogenic conditions (Figure 11C). The overall appearance of the fracture surface of the CFRP-VI resin laminates (Figure 11B) closely resembled that of the CFRP-CC laminates, which further supports the similarity in the measured G_{IIc} values.

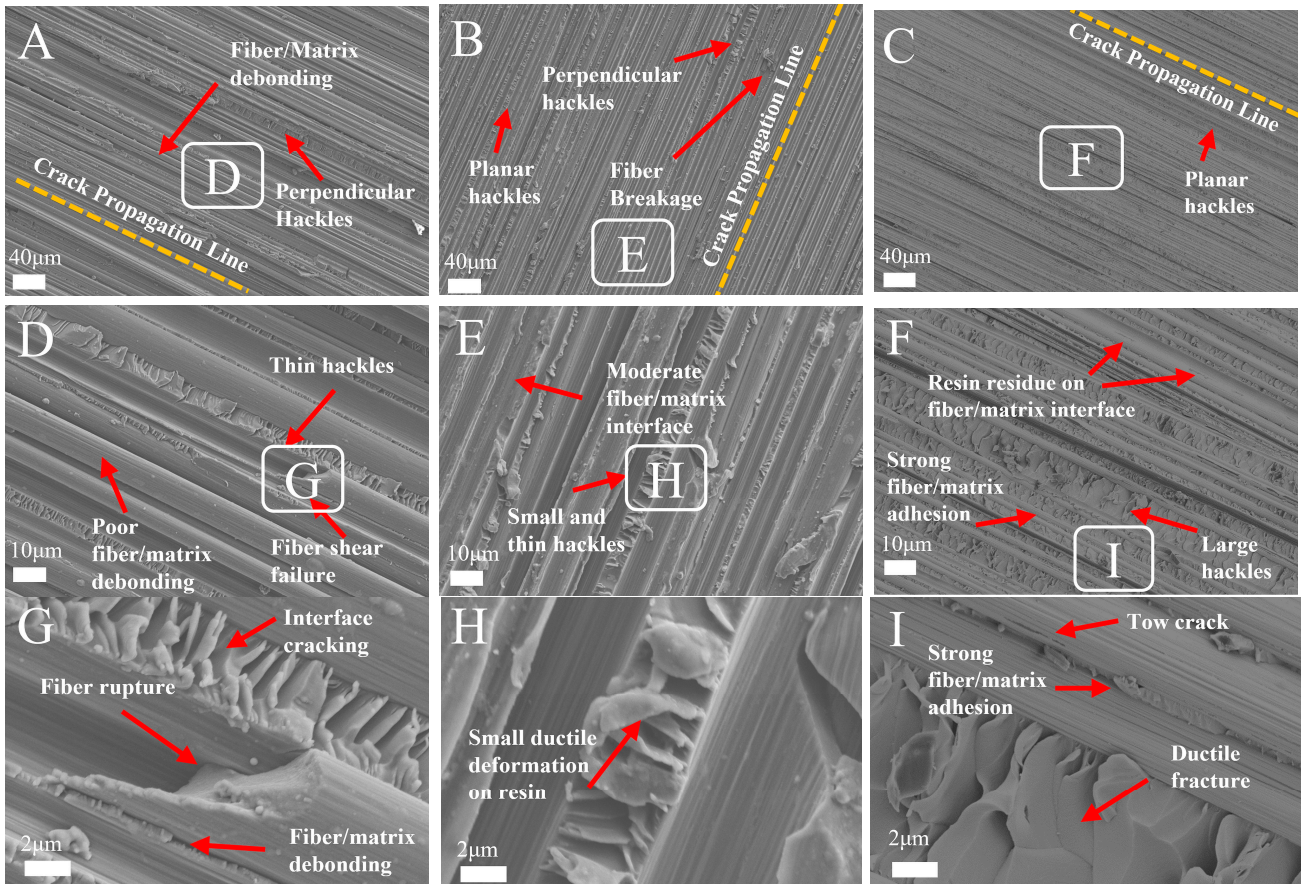


Figure 11. Fracture surfaces of cryogenic fractured filament wound UD (0)₁₆ laminates with (A,D,G) CFRP-CC resin, (B,E,H) CFRP-VI resin and (C,F,I) CFRP-T resin.

When zoomed in (Figure 11D,E), a notable shift in the resin morphologies for the CC resin and VI resin was evident under cryogenic conditions. In this context, the fiber/matrix interfaces displayed smaller and thinner hackles, a consequence of the brittleness effect [46]. Conversely, the dominance of resin damage was apparent for the T resin system, indicating the contribution of the resin to the G_{IIc} values under cryogenic conditions (Figure 11F). An enhanced quality of fiber/matrix bonding was once again observed in the CFRP-VI resin and CFRP-T resin laminates. This was particularly relevant for the cryogenic fracture of the laminates, as the primary mode of failure was associated with fiber/matrix debonding. Notably, the toughened CFRP-T resin still showed large fractured ductile hackles under cryogenic conditions, alongside strong fiber/matrix adhesion. This explains the equivalent G_{IIc} values obtained between the RT and LN2 conditions for this resin system.

When further zoomed in, the shape of the hackles on the CFRP-CC resin laminate unveiled an example failure mode unique to the cryogenic testing. This mode involved in fiber/matrix interface cracking and fiber shear rupture (Figure 11G) due to the extreme cold and large difference in the thermal expansion coefficients between the constituents [10]. This situation may have caused a self-cracking event prior to the loading, potentially leading to a reduction in the G_{IIc} values. This failure mode was not observed in the CFRP-VI resin and CFRP-T resin laminates, where better fiber/matrix adhesion was achieved. In the case

of the CFRP-T resin system, the strong fiber/matrix adhesion resulted in tow cracking and splitting on the fiber (Figure 11I). Furthermore, the ductile resin failure morphology revealed the cryogenic performance capability of this resin system (Figure 11I).

5. Conclusions

The mode-II delamination behavior of filament-wound CFRP laminates with different resin types was extensively investigated under both room-temperature and cryogenic conditions by employing a detailed fractographic analysis. Notably, the G_{IIc} values of the CC resin system exhibited a significant reduction, decreasing from 1.74 ± 0.17 (kJ/m²) at room temperature to 0.88 ± 0.05 (kJ/m²) at cryogenic temperature. In contrast, both the VI and T resin systems displayed relatively stable G_{IIc} values between room and cryogenic temperature. The measured G_{IIc} values of the VI resin were 0.97 ± 0.21 (kJ/m²) at room temperature and 0.94 ± 0.08 (kJ/m²) at cryogenic temperature. The G_{IIc} values for the T resin system were 1.268 ± 0.091 (kJ/m²) under room-temperature conditions and 1.216 ± 0.121 (kJ/m²) under cryogenic conditions. The following conclusions were drawn based on the experimental findings of this study:

- The three-point bending tests on the neat epoxy specimens demonstrated that cryogenic temperatures led to a decrease in the elongation and an increase in the strength and stiffness due to embrittlement. It became apparent that the neat epoxy's performance may not accurately reflect the cryogenic performance of the composites due to the dominant influence of fiber/matrix interactions on the damage behavior. Consequently, experimental efforts focusing on single-fiber tow/resin interactions may be favored.
- The mode-II delamination behavior was notably affected by inherent resin bagging and tow undulation problems associated with conventional wet winding. Their presence caused complex 3D crack propagation. Tow movement at room temperature provided resin ductility, contributing to an increase in the G_{IIc} levels through a tow interlocking mechanism.
- Matrix shear failure, fiber/matrix debonding and even fiber fracture events were observed during crack propagation at room temperature.
- Under cryogenic temperatures, the dominant failure mode shifted towards fiber/matrix debonding, characterized by visible zig-zag crack propagation, as seen from side views of the specimens.
- The VI resin, with the lowest mixture viscosity, suffered from a wetting problem that increased the contribution of the undulated fiber architecture (tow interlocking). This mechanism explained the similar G_{IIc} values measured at both room and cryogenic temperatures, with the embrittlement events observed for the neat resin system having a limited impact on the laminate behavior.
- The CC resin system, with a moderate mixture viscosity, enabled better wetting of the interlaminar plane. This was associated with the pre-crack insertion process, where the overall winding process was temporarily halted. The combination of the undulated fiber architecture and matrix phase contributed to the highest G_{IIc} levels measured at room temperature. However, this case also experienced the most significant G_{IIc} reduction under cryogenic temperatures, which may be attributed to resin embrittlement. The fractographic analyses suggested that nanoscale matrix cracking, fiber shear fracturing and fiber/matrix debonding events collectively contributed the ultimate fracture.
- The T resin system, with the highest mixture viscosity, likewise offered good wetting. Parallel to the VI resin system, the G_{IIc} values of the T resin system remained stable under cryogenic conditions. The fractographic analyses indicated better fiber/matrix adhesion under cryogenic temperatures. This fact simultaneously allowed for an equal contribution of the matrix phase during mode-II crack propagation. Notably, typical shear hackles inherent to mode-II crack propagation were observed on the fracture surfaces of the samples tested under cryogenic conditions. This situation was not

present in any of the other resins due to the fact that the damage progression under cryogenic temperatures was always initiated by fiber/matrix debonding followed by other failure events.

In summary, the reported results and conclusions underline the key considerations related to material selection and manufacturing-related issues that influence the performance of filament-wound laminates under cryogenic conditions. Although such problems may be overcome by the use of more advanced AFP techniques, the presented interpretation of the delamination behavior of wet-wound laminates may provide guidance for further material development. With such efforts, pressure vessels with limited operational lifetimes (e.g., sounding rockets) could still be efficiently manufactured through conventional filament winding, a method that remains a dominant and cost-effective manufacturing approach in terms of volume.

Author Contributions: Conceptualization, R.U., K.B., M.E. and A.K.; Data curation, R.U. and K.B.; Formal analysis, R.U., K.B. and B.E.K.; Funding acquisition, M.E. and A.K.; Investigation, R.U., K.B. and B.E.K.; Methodology, R.U. and K.B.; Project administration, M.E. and A.K.; Resources, R.U., K.B., B.E.K. and A.K.; Software, K.B. and B.E.K.; Supervision, M.E. and A.K.; Validation, R.U., K.B. and B.E.K.; Visualization, R.U. and K.B.; Writing—original draft, R.U. and K.B.; Writing—review and editing, R.U., K.B., M.E. and A.K. All authors have read and agreed to the published version of the manuscript.

Funding: This research received no external funding.

Data Availability Statement: Data are unavailable due to privacy.

Acknowledgments: The authors greatly acknowledged DeltaV Space Technologies Inc. for their financial support and for providing research facilities during the realization of this study.

Conflicts of Interest: The authors declare no conflict of interest.

References

1. Abumeri, G.H.; Kosareo, D.N.; Roche, J.M. Cryogenic Composite Tank Design for next Generation Launch Technology. In Proceedings of the 40th AIAA/ASME/SAE/ASEE Joint Propulsion Conference and Exhibit, Fort Lauderdale, FL, USA, 11–14 July 2004.
2. Mallick, K.; Cronin, J.; Ryan, K.; Arzberger, S.; Munshi, N.; Paul, C.; Welsh, J.S. An Integrated Systematic Approach to Linerless Composite Tank Development. In Proceedings of the Collection of Technical Papers—46th AIAA/ASME/ASCE/AHS/ASC Structures, Structural Dynamics and Materials Conference, Austin, TX, USA, 18–21 April 2005; Volume 5, pp. 3553–3569.
3. Chen, D.; Li, J.; Yuan, Y.; Gao, C.; Cui, Y.; Li, S.; Liu, X.; Wang, H.; Peng, C.; Wu, Z. A Review of the Polymer for Cryogenic Application: Methods, Mechanisms and Perspectives. *Polymers* **2021**, *13*, 320. [[CrossRef](#)] [[PubMed](#)]
4. Adams, D.S.; Bowles, D.E.; Herakovich, C.T. Thermally Induced Transverse Cracking in Graphite-Epoxy Cross-Ply Laminates. *J. Reinf. Plast. Compos.* **1986**, *5*, 152–169. [[CrossRef](#)]
5. Bechel, V.T.; Kim, R.Y. Damage Trends in Cryogenically Cycled Carbon/Polymer Composites. *Compos. Sci. Technol.* **2004**, *64*, 1773–1784. [[CrossRef](#)]
6. Nguyen, B.N.; Simmons, K.L. A Multiscale Modeling Approach to Analyze Filament-Wound Composite Pressure Vessels. *J. Compos. Mater.* **2013**, *47*, 2113–2123. [[CrossRef](#)]
7. Pereira, A.B.; De Morais, A.B. Mode II Interlaminar Fracture of Glass/Epoxy Multidirectional Laminates. *Compos. Part A Appl. Sci. Manuf.* **2004**, *35*, 265–272. [[CrossRef](#)]
8. Choi, S.; Sankar, B.V. Micromechanical Analysis of Composite Laminates at Cryogenic Temperatures. *J. Compos. Mater.* **2006**, *40*, 1077–1091. [[CrossRef](#)]
9. Azeem, M.; Ya, H.H.; Kumar, M.; Stabla, P.; Smolnicki, M.; Gemi, L.; Khan, R.; Ahmed, T.; Ma, Q.; Sadique, M.R.; et al. Application of Filament Winding Technology in Composite Pressure Vessels and Challenges: A Review. *J. Energy Storage* **2022**, *49*, 103468. [[CrossRef](#)]
10. Shindo, Y.; Takeda, T.; Narita, F.; Saito, N.; Watanabe, S.; Sanada, K. Delamination Growth Mechanisms in Woven Glass Fiber Reinforced Polymer Composites under Mode II Fatigue Loading at Cryogenic Temperatures. *Compos. Sci. Technol.* **2009**, *69*, 1904–1911. [[CrossRef](#)]
11. Flanagan, M.; Grogan, D.M.; Goggins, J.; Appel, S.; Doyle, K.; Leen, S.B.; Ó Brádaigh, C.M. Permeability of Carbon Fibre PEEK Composites for Cryogenic Storage Tanks of Future Space Launchers. *Compos. Part A Appl. Sci. Manuf.* **2017**, *101*, 173–184. [[CrossRef](#)]

12. Grogan, D.M.; Ó Brádaigh, C.M.; McGarry, J.P.; Leen, S.B. Damage and Permeability in Tape-Laid Thermoplastic Composite Cryogenic Tanks. *Compos. Part A Appl. Sci. Manuf.* **2015**, *78*, 390–402. [[CrossRef](#)]
13. Yokozeki, T.; Ogasawara, T.; Aoki, T.; Ishikawa, T. Experimental Evaluation of Gas Permeability through Damaged Composite Laminates for Cryogenic Tank. *Compos. Sci. Technol.* **2009**, *69*, 1334–1340. [[CrossRef](#)]
14. Nishijima, S.; Honda, Y.; Okada, T. Application of the Positron Annihilation Method for Evaluation of Organic Materials for Cryogenic Use. *Cryogenics* **1995**, *35*, 779–781. [[CrossRef](#)]
15. Pozdnyakov, A.O.; Brzhezinskaya, M.M.; Vinogradov, A.S.; Friedrich, K. NEXAFS Spectra of Polymer-Nanocarbon Composites. In Proceedings of the Fullerenes Nanotubes and Carbon Nanostructures, Phoenix, AZ, USA, 18–23 May 2008; Volume 16.
16. Shen, X.J.; Liu, Y.; Xiao, H.M.; Feng, Q.P.; Yu, Z.Z.; Fu, S.Y. The Reinforcing Effect of Graphene Nanosheets on the Cryogenic Mechanical Properties of Epoxy Resins. *Compos. Sci. Technol.* **2012**, *72*, 1581–1587. [[CrossRef](#)]
17. He, Y.; Zhang, L.; Chen, G.; Li, X.; Yao, D.; Lee, J.H.; Zhang, Y. Surface Functionalized Carbon Nanotubes and Its Effects on the Mechanical Properties of Epoxy Based Composites at Cryogenic Temperature. *Polym. Bull.* **2014**, *71*, 2465–2485. [[CrossRef](#)]
18. Tudela, M.; Kim, R. Impact Damage Response of Composite Materials at LOX/Cryogenic Temperatures. In Proceedings of the Collection of Technical Papers—AIAA/ASME/ASCE/AHS/ASC Structures, Structural Dynamics and Materials Conference, Austin, TX, USA, 18–21 April 2005; Volume 7.
19. Liu, X.; Sun, T.; Wu, Z.; He, H. Mode II Interlaminar Fracture Toughness of Unidirectional Fiber-Reinforced Polymer Matrix Composites with Synthetic Boehmite Nanosheets at Room Temperature and Low Temperature. *J. Compos. Mater.* **2018**, *52*, 945–952. [[CrossRef](#)]
20. Zhao, Y.; Chen, Z.K.; Liu, Y.; Xiao, H.M.; Feng, Q.P.; Fu, S.Y. Simultaneously Enhanced Cryogenic Tensile Strength and Fracture Toughness of Epoxy Resins by Carboxylic Nitrile-Butadiene Nano-Rubber. *Compos. Part A Appl. Sci. Manuf.* **2013**, *55*, 178–187. [[CrossRef](#)]
21. Kim, B.C.; Park, S.W.; Lee, D.G. Fracture Toughness of the Nano-Particle Reinforced Epoxy Composite. *Compos. Struct.* **2008**, *86*, 69–77. [[CrossRef](#)]
22. Coronado, P.; Argüelles, A.; Viña, J.; Viña, I. Influence of Low Temperatures on the Phenomenon of Delamination of Mode I Fracture in Carbon-Fibre/Epoxy Composites under Fatigue Loading. *Compos. Struct.* **2014**, *112*, 188–193. [[CrossRef](#)]
23. Bechel, V.T.; Negilski, M.; James, J. Limiting the Permeability of Composites for Cryogenic Applications. *Compos. Sci. Technol.* **2006**, *66*, 2284–2295. [[CrossRef](#)]
24. Rousseau, J.; Perreux, D.; Verdrière, N. The Influence of Winding Patterns on the Damage Behaviour of Filament-Wound Pipes. *Compos. Sci. Technol.* **1999**, *59*, 1439–1449. [[CrossRef](#)]
25. Torres Arellano, M.; Crouzeix, L.; Douchin, B.; Collombet, F.; Hernández Moreno, H.; González Velázquez, J. Strain Field Measurement of Filament-Wound Composites at $\pm 55^\circ$ Using Digital Image Correlation: An Approach for Unit Cells Employing Flat Specimens. *Compos. Struct.* **2010**, *92*, 2457–2464. [[CrossRef](#)]
26. Hernández-Moreno, H.; Douchin, B.; Collombet, F.; Choqueuse, D.; Davies, P. Influence of Winding Pattern on the Mechanical Behavior of Filament Wound Composite Cylinders under External Pressure. *Compos. Sci. Technol.* **2008**, *68*, 1015–1024. [[CrossRef](#)]
27. Zhang, Y.; Xia, Z.; Ellyin, F. Two-Scale Analysis of a Filament-Wound Cylindrical Structure and Application of Periodic Boundary Conditions. *Int. J. Solids Struct.* **2008**, *45*, 5322–5336. [[CrossRef](#)]
28. Mian, H.H.; Rahman, H. Influence of Mosaic Patterns on the Structural Integrity of Filament Wound Composite Pressure Vessels. *Int. J. Struct. Integr.* **2011**, *2*, 345–356. [[CrossRef](#)]
29. Pai, S.P.; Jensen, D.W. Influence of Fiber Undulations on Buckling of Thin Filament-Wound Cylinders in Axial Compression. *J. Aerosp. Eng.* **2001**, *14*, 12–20. [[CrossRef](#)]
30. Pourahmadi, E.; Taheri-Behrooz, F. The Influence of Fiber Bundle Width on the Mechanical Properties of Filament-Wound Cylindrical Structures. *Int. J. Mech. Sci.* **2020**, *178*, 105617. [[CrossRef](#)]
31. Shen, C.; Han, X. Damage and Failure Analysis of Filament Wound Composite Structure Considering Fibre Crossover and Undulation. *Adv. Compos. Lett.* **2018**, *27*, 55–70. [[CrossRef](#)]
32. Barcikowski, M.; Rybkowska, K. Mode II Fracture Characterization of Toughened Epoxy Resin Composites. *Int. J. Fract.* **2022**, *234*, 223–233. [[CrossRef](#)]
33. Abd Rased, M.F.; Yoon, S.H. Experimental Study on Effects of Asymmetrical Stacking Sequence on Carbon Fiber/Epoxy Filament Wound Specimens in DCB, ENF, and MMB Tests. *Compos. Struct.* **2021**, *264*, 113749. [[CrossRef](#)]
34. De Moraes, A.B.; Silva, J.F.; Marques, A.T.; De Castro, P.T. Mode II Interlaminar Fracture of Filament Wound Angle-Ply Specimens. *Appl. Compos. Mater.* **2002**, *9*, 117–129. [[CrossRef](#)]
35. Bonhomme, J.; Argüelles, A.; Viña, J.; Viña, I. Fractography and Failure Mechanisms in Static Mode I and Mode II Delamination Testing of Unidirectional Carbon Reinforced Composites. *Polym. Test.* **2009**, *28*, 612–617. [[CrossRef](#)]
36. Li, S.; Chen, D.; Yuan, Y.; Gao, C.; Cui, Y.; Wang, H.; Liu, X.; Liu, M.; Wu, Z. Influence of Flexible Molecular Structure on the Cryogenic Mechanical Properties of Epoxy Matrix and Carbon Fiber/Epoxy Composite Laminate. *Mater. Des.* **2020**, *195*, 109028. [[CrossRef](#)]
37. Choi, S.; Sankar, B.V. Fracture Toughness of Transverse Cracks in Graphite/Epoxy Laminates at Cryogenic Conditions. *Compos. Part B Eng.* **2007**, *38*, 193–200. [[CrossRef](#)]
38. ASTM D790-17; Standard Test Methods for Flexural Properties of Unreinforced and Reinforced Plastics and Electrical Insulating Materials. ASTM International: West Conshohocken, PA, USA, 2002; pp. 1–12.

39. ASTM D7905; Standard Test Method for Determination of the Mode II Interlaminar Fracture Toughness of Unidirectional Fiber-Reinforced Polymer Matrix Composites. ASTM International: West Conshohocken, PA, USA, 2014; pp. 1–18.
40. ISO 1268-5; Fibre-Reinforced Plastics—Methods of Producing Test Plates—Part 5: Filament Winding. ISO (International Organization for Standardization): Geneva, Switzerland, 2015; Volume 10406-1:20, pp. 3–6.
41. Srivastava, V.K.; Gries, T.; Veit, D.; Quadflieg, T.; Mohr, B.; Kolloch, M. Effect of Nanomaterial on Mode I and Mode II Interlaminar Fracture Toughness of Woven Carbon Fabric Reinforced Polymer Composites. *Eng. Fract. Mech.* **2017**, *180*, 73–86. [[CrossRef](#)]
42. Peng, C.; Li, J.; Wu, Z.; Peng, W.; Zhou, D. Investigating into the Liquid Oxygen Compatibility of a Modified Epoxy Resin Containing Silicon/Phosphorus and Its Mechanical Behavior at Cryogenic Temperature. *RSC Adv.* **2016**, *6*, 38300–38309. [[CrossRef](#)]
43. Feng, Q.; Yang, J.; Liu, Y.; Xiao, H.; Fu, S. Simultaneously Enhanced Cryogenic Tensile Strength, Ductility and Impact Resistance of Epoxy Resins by Polyethylene Glycol. *J. Mater. Sci. Technol.* **2014**, *30*, 90–96. [[CrossRef](#)]
44. Ward, I.M.; Pinnock, P.R. The Mechanical Properties of Solid Polymers. *Br. J. Appl. Phys.* **1966**, *17*, 3–32. [[CrossRef](#)]
45. Chu, X.X.; Wu, Z.X.; Huang, R.J.; Zhou, Y.; Li, L.F. Mechanical and Thermal Expansion Properties of Glass Fibers Reinforced PEEK Composites at Cryogenic Temperatures. *Cryogenics* **2010**, *50*, 84–88. [[CrossRef](#)]
46. Johannesson, T.; Sjöblom, P.; Seldén, R. The Detailed Structure of Delamination Fracture Surfaces in Graphite/Epoxy Laminates. *J. Mater. Sci.* **1984**, *19*, 1171–1177. [[CrossRef](#)]
47. Wang, Z.; Almeida, J.H.S.; St-Pierre, L.; Wang, Z.; Castro, S.G.P. Reliability-Based Buckling Optimization with an Accelerated Kriging Metamodel for Filament-Wound Variable Angle Tow Composite Cylinders. *Compos. Struct.* **2020**, *254*, 112821. [[CrossRef](#)]
48. Koschmieder, M.; Michaeli, W. On-Line Tow Width Measurement in Filament Winding. *Int. SAMPE Symp. Exhib.* **2000**, *45*, 1417.

Disclaimer/Publisher’s Note: The statements, opinions and data contained in all publications are solely those of the individual author(s) and contributor(s) and not of MDPI and/or the editor(s). MDPI and/or the editor(s) disclaim responsibility for any injury to people or property resulting from any ideas, methods, instructions or products referred to in the content.